Undrained capacity of shallow octagonal foundations under combined VHM loading

He, Pengpeng; Deshpande, Venkatesh; Newson, Tim

Published in:
Geotechnical and Geological Engineering

DOI:
10.1007/s10706-022-02334-z

Publication date:
2022

Document Version
Peer reviewed version

Geotechnical and Geological Engineering

Undrained capacity of shallow octagonal foundations under combined VHM loading

--Manuscript Draft--

Manuscript Number:	GEGE-D-22-00087R2
Full Title:	Undrained capacity of shallow octagonal foundations under combined VHM loading
Article Type:	Original Paper
Keywords:	Octagonal foundation; Zero-tension interface; Failure envelope; finite element analysis; Combined loading
Corresponding Author:	Pengpeng He, Ph.D. Western University London, Ontario CANADA
Corresponding Author Secondary Information:	
Corresponding Author's Institution:	Western University
Corresponding Author's Secondary Institution:	
First Author:	Pengpeng He, Ph.D.
First Author Secondary Information:	
Order of Authors:	Pengpeng He, Ph.D. Venkatesh Deshpande Tim Newson, Ph.D., Professor
Order of Authors Secondary Information:	
Funding Information:	Natural Sciences and Engineering Research Council of Canada (RGPIN-2015-06062) — Dr. Tim Newson
Abstract:	The foundations of many large onshore and offshore structures are designed to be symmetrical polygons (e.g. octagons). However, the available analytical approaches for the ultimate limit state design of shallow foundations under combined loadings focus predominately on strip, rectangular and circular foundations. Although equivalent inscribed circular foundations have been recommended for foundation design by some guidelines, this simple approximation for octagonal foundations needs to be rigorously assessed due to the high dependence of the failure envelope on foundation shapes. The present study has investigated the general VHM (vertical, horizontal and moment) failure envelope of octagonal foundations under a zero-tension interface for undrained soil conditions using finite element analysis. The effects of soil strength heterogeneity and foundation embedment on the VHM failure envelope have been investigated. Analytical expressions have also been proposed to characterize the failure envelopes for use in design. The results show that octagonal foundations have larger bearing capacity than the corresponding circular foundations, and the difference (around 10%) between them is not negligible. A full 3-D analytical expression for the VHM failure envelope has also been proposed based on the calculated failure envelopes.
Response to Reviewers:	Dear Editors and Reviewers: We have put the response letter in first section of the revised manuscript, as we we did not see a space for a separate response letter document (which contains some figures) in the online submission system. We hope that this is fine with you. Thanks. Best wishes, Pengpeng He

Response Letter

Dear Editors and Reviewers:

We appreciate your time and helpful comments. We believe all of the comments have been suitably addressed. The comments are immensely beneficial for increasing the quality of the manuscript and to enable it to be considered as a full paper in your esteemed journal. Our response to the first reviewer's comments is given below.

Reviewer #1:

1. I am still not convinced this is a worthwhile contribution to the journal. Nevertheless the authors have made a good attempt in addressing the questions from the two reviewers. Both the reviewers raised the question on the E/s_u ratio used by the authors. Their answer is not satisfactory. They used 10000, which is unrealistically high. In any case, without validation data, this cannot go as a full paper. Possibly a technical note after it is shortened significantly.

Octagonal foundations have been widely used for onshore wind turbines in North America, yet have not been well addressed in the literature. DNV (2016) recommends an equivalent inscribed circular foundation for the design of foundations shaped as a double symmetrical polygon (octagonal or more), but there is still no theoretical (or any other) validation for this assumption. In addition, as you observed from our paper, an octagonal foundation has about 10% greater bearing capacity than the inscribed circular foundation suggested by DNV (2016). We believe that this difference can provide additional margins of safety and given the significant number of foundations on typical wind farms provides impactful economics of scale. Hence, we believe this paper is a worthy contribution to your journal and given the paucity of information on these foundations, should be highly cited.

We agree that the ratio of E/s_u=10000 used in the paper is unrealistically large, but this high ratio does not affect the failure envelopes investigated in this paper. On the other hand, a higher ratio significantly reduces the distortion of mesh elements close to the soil-foundation interface, which

can help avoid non-convergence issues caused by excessive mesh distortion. The ratio of E/s_u=10000 has also been used in some of our other publications (He and Newson, 2022(a); 2022(b)). In addition, Abyaneh et al. (2015) has shown that the bearing capacities of square foundations are independent of the rigidity index (i.e., G/s_u). It is also found that a higher rigidity index results in the failure at smaller deformations and helps minimize numerical issues associated with mesh distortion. Although Abyaneh et al. (2015) only presents the uniaxial bearing capacities (V_{ult}, H_{ult}, and M_{ult}) of square foundations for the cases of relatively smaller values of G/s_u=80 and 335 (i.e., E/s_u=240 and 1005), the effect of E/s_u is believed to remain the same for octagonal foundations with greater E/s_u values.

In order to show the effect of E/s_u ratios, we have carried out additional finite element analyses (FEA) which are shown below. In the analysis, we took a surface octagonal foundation on a homogeneous soil as an example, and three E/s_u ratios have been chosen, that is, E/s_u=10000, 5000 and 1000. The original data obtained from the FEA are compared in the figures below.

Figure 1 shows the relationship between the vertical load and vertical displacement of the foundation calculated by FEA. Since there are no plateaus for the curves, the tangent intersection point method (intersection between the initial and post-yield tangent lines) is used to determine the failure loads, as shown in Figure 1. The derived ultimate vertical loads for E/s_u=10000, 5000 and 1000 are V/As_u=6.54, 6.53 and 6.47 (differences within 1.2%), respectively. This implies that the effect of E/s_u on the vertical ultimate capacity is negligible.

The comparison also shows that the ratio affects mainly the evolution of the curve, particularly the initial stiffness of the curve. A lower E/s_u ratio results in a smaller initial stiffness and a greater vertical displacement to achieve the bearing capacity, which may cause excessive mesh distortion and model non-convergence in some cases. The mesh deformations around the foundation corner at failure are compared in Figure 2. It can be seen that the soil elements close to the foundation edges for the case of E/s_u=1000 are much more significantly distorted than those for the case of E/s_u=10000.

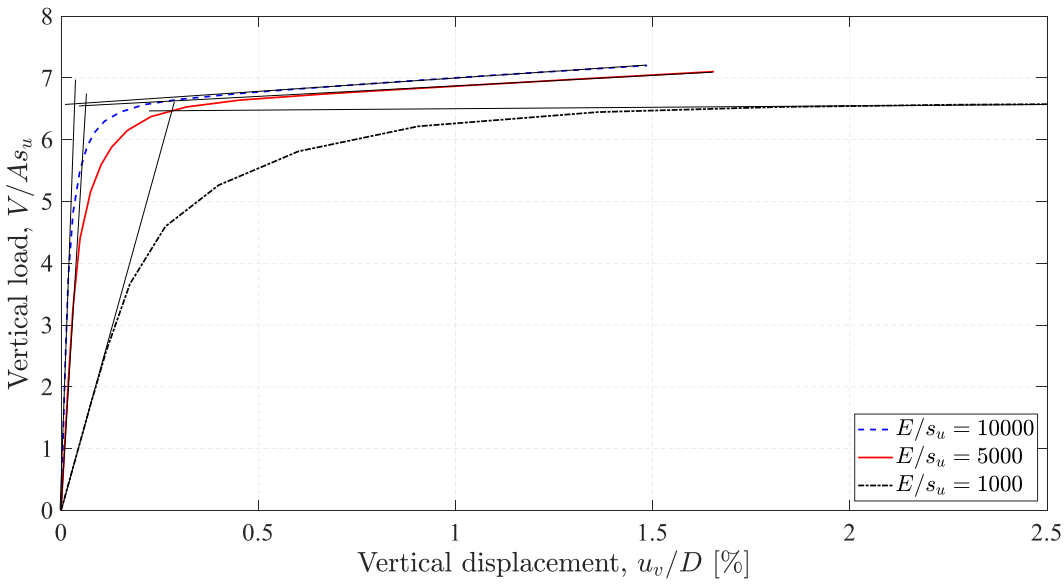

Figure 1. Vertical load versus vertical displacement of the foundation

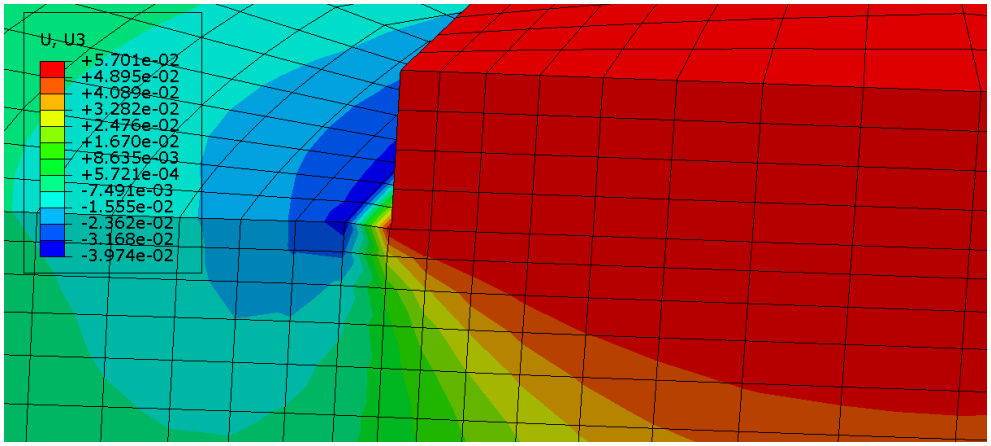

(a) E/s_u=10000

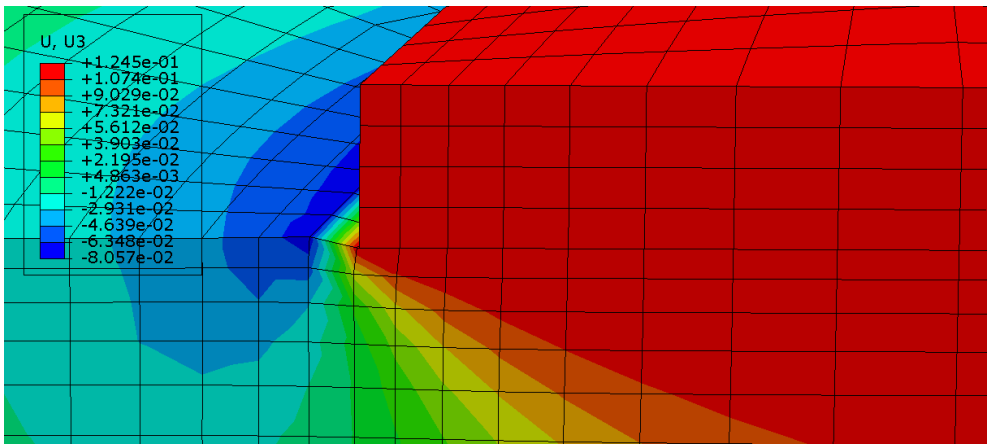

(b) E/s_u=5000

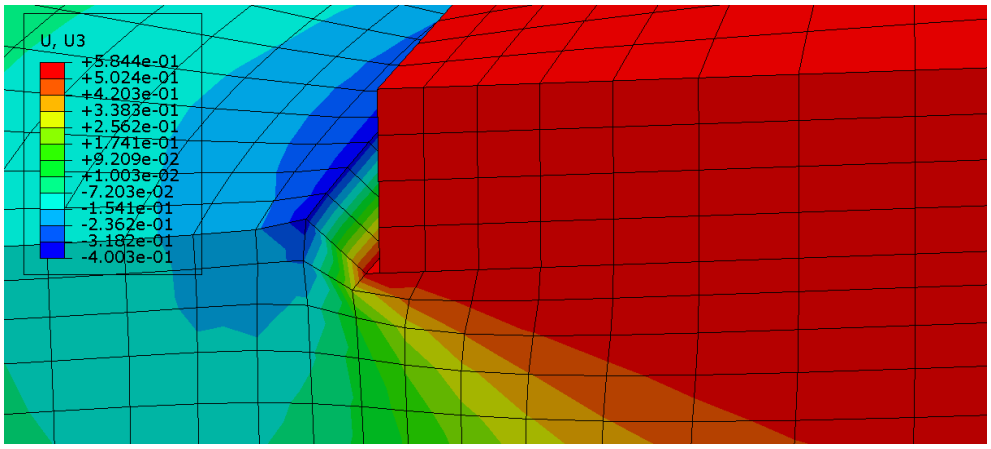

(c) E/s_u=1000

Figure 2. Mesh deformations at failure

Figure 3 shows the relationship between the horizontal load and displacement of the foundation calculated by FEA. Apparently, the three cases achieve the same horizontal capacity although the initial stiffness of the curves differs.

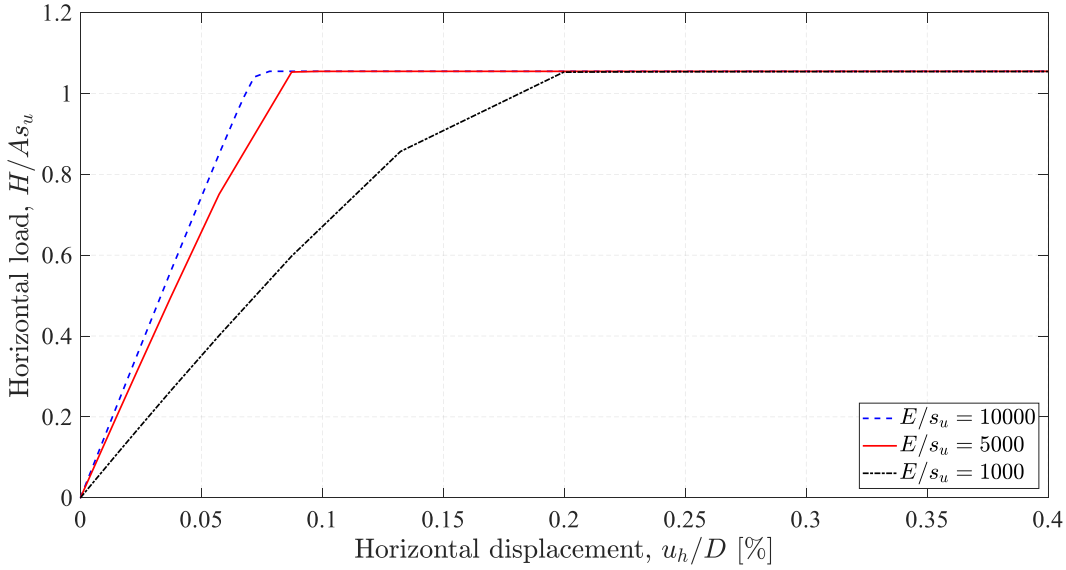

Figure 3. Horizontal load versus horizontal displacement of the foundation

Figure 4 shows the relationship between the moment and rotation of the foundation obtained by FEA. Similar to the vertical capacity shown in Figure 1, the calculated moment capacities corresponding to E/s_u=10000, 5000 and 1000 are M/ADs_u=0.71, 0.70 and 0.69 (differences within 3%). Thus, the E/s_u ratio has a very limited effect on the moment capacity although the ratio also has a great influence on the evolution of the curve.

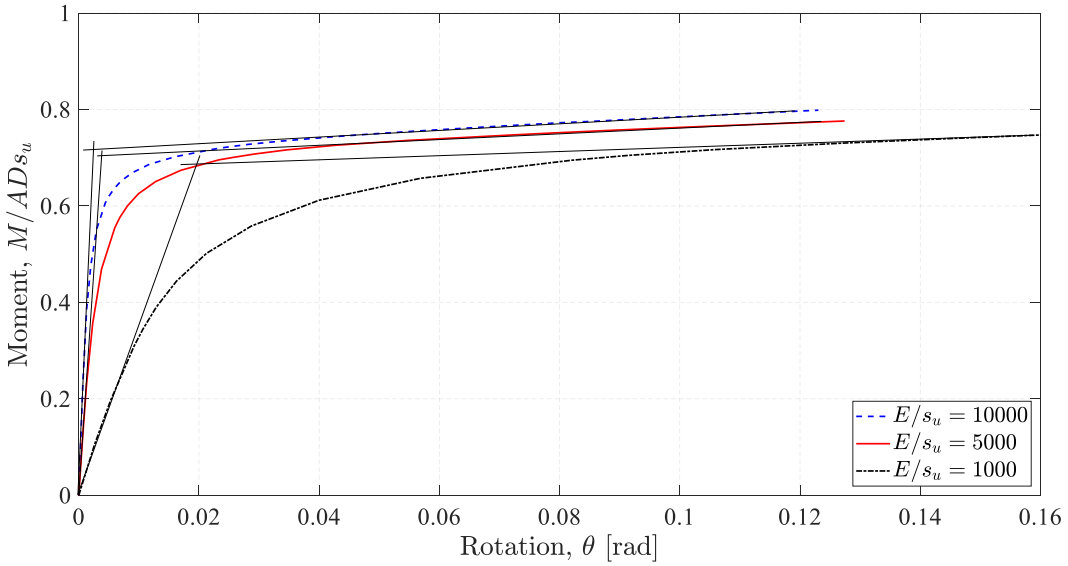

Figure 4. Moment versus rotation of the foundation

Figure 5 shows the relationship between the horizontal load and moment on the foundation for the case of $u_h/\theta D$=1.0 (displacement-controlled) at V/V_{ult}=0.5 calculated by FEA. The FEA results are also compared to the *M-H* envelope. It can be seen that the three cases lead to different loci on the same *M-H* envelope. This means that FEA using different E/s_u ratios will result in the same *M-H* envelope. Hence the E/s_u ratio has a negligible effect on the calculated *M-H* envelope.

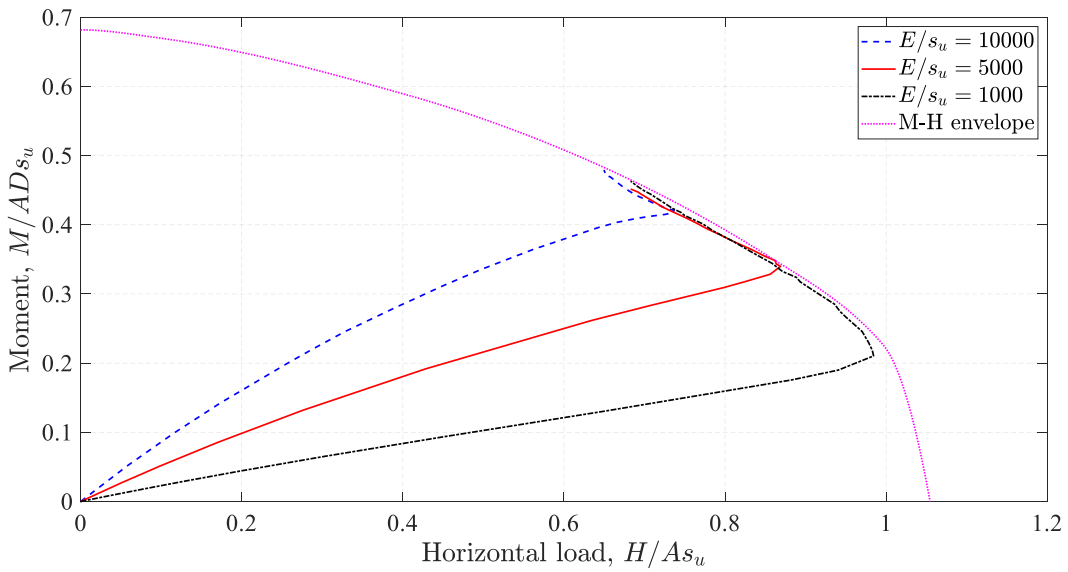

Figure 5. Moment versus horizontal load on the foundation

Finally, with respect to the comments regarding validation, as stated previously it would certainly be of benefit for future lab scale and field scale complementary testing be conducted. Since this is a numerical study, this is beyond the scope of this work and we believe that validation against the robust previously peer-reviewed FEA of circular foundations is sufficient in the absence of theoretical solutions or field/lab tests (which have inherent problems too). If this requirement was applied to all papers in our field, there would be a lot less publications in the literature.

We look forward to hearing from you and the reviewers in due course about the revised paper.

Best wishes,

Tim Newson

References

He P, Newson T (2022a) Undrained capacity of circular shallow foundations on two-layer clays under combined VHMT loading. Canadian Geotechnical Journal, 59(8), 1523-1526.

He P, Newson T (2022b) Undrained capacity of circular shallow foundations under combined VHMT loading. Wind Engineering, 46(5), 1452-1470.

Abyaneh SD, Ojo A, Maconochie A, Haghighi A (2015) The undrained bearing capacity of shallow foundations subjected to three-dimensional loading including torsion. In Proceedings of the 25th International Ocean and Polar Engineering Conference, Kona, Hawaii, 21-26 June 2015. International Society of Offshore and Polar Engineers, Cupertino, pp. 668-674.

DNV GL, DNVGL-ST-0126 (2016) Support structures for wind turbines. DNV GL, Oslo, Norway.

Undrained capacity of shallow octagonal foundations under combined VHM loading

Pengpeng He, Ph.D. Geotechnical Research Centre, Department of Civil & Environmental Engineering, Western University, London, Canada. Email: phe27@uwo.ca

Venkatesh Deshpande, Ph.D. candidate. Indian Institute of Technology, Delhi, India. Email: venkateshmdeshpande@gmail.com

Tim Newson, Ph.D., Associate Prof. Geotechnical Research Centre, Department of Civil & Environmental Engineering, Western University, London, Canada. Email: tnewson@eng.uwo.ca

Corresponding author:

Pengpeng He, Ph.D.

Geotechnical Research Centre, Department of Civil & Environmental Engineering, Western University, London, Canada

Email: phe27@uwo.ca

Tel: (+1) 519-697-8206

Word count: 3821 (texts) + (14+0)×250 = 7321 (14 figures and 0 tables, including captions but excluding this title page)

Abstract: The foundations of many large onshore and offshore structures are designed to be symmetrical polygons (e.g. octagons). However, the available analytical approaches for the ultimate limit state design of shallow foundations under combined loadings focus predominately on strip, rectangular and circular foundations. Although equivalent inscribed circular foundations have been recommended for foundation design by some guidelines, this simple approximation for octagonal foundations needs to be rigorously assessed due to the high dependence of the failure envelope on foundation shapes. The present study has investigated the general VHM (vertical, horizontal and moment) failure envelope of octagonal foundations under a zero-tension interface for undrained soil conditions using finite element analysis. The effects of soil strength heterogeneity and foundation embedment on the VHM failure envelope have been investigated. Analytical expressions have also been proposed to characterize the failure envelopes for use in design. The results show that octagonal foundations have larger bearing capacity than the corresponding circular foundations, and the difference (around 10%) between them is not negligible. A full 3-D analytical expression for the VHM failure envelope has also been proposed based on the calculated failure envelopes.

Keywords: Octagonal foundation; Zero-tension interface; Failure envelope; Finite element analysis; Combined loading.

1 Introduction

Shallow foundations have been extensively used to support large onshore and offshore structures, such as wind turbines, platforms, transmission towers and masts. The bearing capacity of their shallow foundations under combined loadings is particularly important. For example, the horizontal loads on an offshore wind turbine caused by combined winds, waves and currents can be substantial, and a large tower height can lead to significant moment loading on the foundation. Traditional analytical methods for these types of foundations are based on classical solutions for the uniaxial vertical bearing capacity of shallow foundations. To account for the effects of load inclination and eccentricity, the load inclination factor and the effective foundation area are introduced, as recommended by some design guidelines (e.g. DNV 2016). However, this approach has been shown to be unconservative for some conditions (Ukritchon et al. 1998), and can be conservative for most cases under combined VHM loadings (Taiebat and Carter 2002).

A more recent design approach is the failure envelope method, which explicitly incorporates the load interaction effects of the various uniaxial loading components (Shen et al. 2017). API (2011) and ISO 19901-4 (2016) recommend this approach as an alternative to conventional theories. Failure envelopes under undrained soil conditions for different foundation geometries, soil strength profiles, and interface conditions have been previously investigated [e.g. strip (Ganesh and Kumar 2021), rectangular (Gourvenec and Randolph 2003) and circular (Suryasentana et al. 2020) foundations; homogeneous strength (Taiebat and Carter 2010) and non-homogeneous strength (Ganesh and Kumar 2021) soils; and zero-tension interface (Shen et al. 2016; He and Newson 2019) and unlimited-tension interface (Wang et al. 2020) conditions] The currently available studies focus primarily on strip, rectangular and circular foundations. Recently, a number of onshore and offshore structures (e.g. wind turbines) have been constructed with foundations that have symmetrical polygon shapes (i.e. octagons) (Yilmaz et al. 2014). DNV (2016) recommends the design of these foundations as an equivalent inscribed circular foundation to accommodate for the octagonal shape. To date, there has been no verification of this assumption (particularly for the failure envelope method). Since the form of the failure envelope for shallow foundations has been found to be highly dependent upon the foundation shape (Gourvenec 2007), this simple approximation for the design of octagonal foundations should hence be rigorously assessed.

Therefore, the object of this study is to investigate the VHM failure envelope for octagonal foundations under a zero-tension interface for undrained soil conditions. The effects of soil strength heterogeneity and foundation embedment

on the VHM failure envelope have been separately studied. A full 3-D VHM failure envelope is proposed using the finite element (FE) method.

2 Method – finite element analysis

2.1 Material models and interface conditions

A linear elastic perfectly plastic constitutive relationship with a Mohr-Coulomb (M-C) failure criterion was used to model the soil behavior. The M-C criterion devolves to the Tresca criterion under undrained soil conditions, which is defined by three soil parameters: the undrained Young's modulus, E_u, the Poisson's ratio, μ, and the undrained shear strength, s_u. In this study, the undrained soil shear strength was considered to linearly increase with depth (z) from the ground surface, as shown in Fig. 1:

$$s_u = s_{u0} + kz \quad (1)$$

where s_{u0} is the undrained shear strength at foundation level; k is the strength increase per unit depth. In the analyses, s_{u0} was held constant at 100 kPa, and the Poisson's ratio of the undrained soil was taken to be 0.495. A sufficiently large E_u/s_{u0} ratio of 10000 was adopted to minimize mesh distortion (Abyaneh et al. 2015). The dimensionless soil strength heterogeneity ratio defined by $\kappa = kD/s_{u0}$ (D is the diameter of the inscribed circle) (Gourvenec and Randolph 2003) was taken as 0 (homogeneous), 2, 6 and 10. The foundation was assumed to act as a rigid body. A load reference point (LRP) attached to the center of the base of foundation was utilized to apply prescribed displacements or loads, as shown in Fig. 1.

Fig. 1 LRP and soil strength profile

A zero-tension rough base that allows separation of the foundation from the soil was considered. As demonstrated by Shen et al. (2016), the zero-tension rough base can be modelled using a Coulomb friction condition with a friction coefficient of 20. For embedded foundations, a reduced friction coefficient (i.e. partially rough interface) for side and top interfaces is recommended due to installation or in-service loading processes (Gourvenec and Mana 2011; Deshpande 2016). In this study, smooth side and top conditions (i.e. an interface adhesion factor α=0 and the shear strength on the interface αs_u=0) for the embedded foundations were considered to provide more conservative predictions. The same consideration was made by Gourvenec and Mana (2011).

2.2 Geometry and mesh

The 3D FE analysis was conducted using the software ABAQUS (Dassault Systèmes 2016). The diameter (D) (inscribed circle) and thickness (t) of the octagonal foundation used in this study are 19 and 3 m, representing typical dimensions for the onshore wind turbines used in North America. The embedment depth ratio, d/D (d refers to the foundation embedment depth), was taken to be 0, 0.08, 0.16, 0.23 and 0.30 to span cases of practical interest to the wind industry. To avoid the effects of the model boundaries, the mesh length, L, and mesh height, H, were taken as 120 and 50 m, following the recommendations of Deshpande (2016).

Fig. 2 Mesh convergence study for a homogeneous soil

Fig. 3 Half-view of the FE mesh

A number of mesh convergence studies were carried out for both surface and embedded foundations, and the result for the case of a surface foundation on a homogeneous soil is shown in Fig. 2. In Fig. 2, V is the vertical load acting on the foundation; A is the soil-foundation contact area; and u_v is the vertical displacement corresponding to V. The difference between the ultimate vertical loads using Mesh 2 (44000 elements) and 3 (79000 elements) is about 3%. However, the model solution with Mesh 3 takes about 2.5 times longer than that using Mesh 2. Therefore, Mesh 2 was adopted in the study. Fig. 3 shows the three-dimensional half model using Mesh 2. The mesh was composed of around 44000 8-noded brick elements (first-order). To capture the intense stress concentration close to the foundation edge and the large plastic shear strains at the interface, the soil regions in the vicinity of the foundation edge and the horizontal thin soil layer close to the interface were carefully refined (Gourvenec and Randolph 2003). The cylindrical circumference of the soil was constrained to prevent out-of-plane translations, and the bottom of the soil domain was fixed in the three orthogonal directions.

2.3 Sign conventions and loading paths

In the analysis, the horizontal and moment loads were considered to be in the same plane. Unlike circular foundations, horizontal and moment loads acting on octagonal foundations can have different loading directions. Since a regular octagon can have planes of symmetry axes, viz. axes passing through the midpoints of two opposite sides (Case I) and axes passing through two opposite vertices (Case II), only these two special loading cases are required for investigations (more general cases lie in between these two extremes), as shown in Fig. 4. Preliminary analyses show that the difference in the failure envelopes between these two loading cases is rather small (less than 5%). Therefore,

only Case I in Fig. 4 was considered for the majority of the analyses. The sign conventions for the loads are shown in Fig. 4.

Fig. 4 Sign conventions

Probe tests were employed to detect the failure envelopes under various loading conditions. In a probe analysis, a vertical load is first applied at the LRP of the foundation and remains constant. A fixed-ratio displacement (see Fig. 5) is then imposed on the foundation to track the failure point on the failure envelope (Gourvenec and Randolph 2003). A probe test can only obtain a single point on a failure envelope. A typical failure envelope obtained using probe tests is shown in Fig. 5.

Fig. 5 *MH* failure envelopes of a surface foundation for κ=0 at V/V_{ult}=0.50

3 Finite element results

This section presents the finite element (FE) results of the pure uniaxial capacities and the failure envelopes (i.e. Horizontal-Vertical, Moment-Vertical and Moment-Horizontal loading) for surface octagonal foundations on heterogenous soils and embedded octagonal foundations in homogeneous soils. The differences between the capacities for octagonal foundations and the corresponding circular foundations are presented.

3.1 Pure uniaxial capacity

The ultimate vertical and horizontal loads are referred to as the corresponding uniaxial load-carrying capacities in the absence of moment loading. As the foundation with a zero-tension interface cannot resist moment loading without vertical loads, the ultimate moment capacity is represented by the maximum moment load only under vertical loading (Shen et al. 2016). The uniaxial bearing capacity factors are defined as:

$$\begin{aligned} v_0 &= V_{\mathrm{ult}}/(A_0 s_{\mathrm{u0}}) \\ h_0 &= H_{\mathrm{ult}}/(A_0 s_{\mathrm{u0}}) \\ m_0 &= M_{\mathrm{ult}}/(A_0 s_{\mathrm{u0}}) \end{aligned} \tag{2}$$

where V_{ult}, H_{ult} and M_{ult} are the uniaxial vertical, horizontal and moment capacities, respectively; A_0 is the area of the inscribed circle of the octagonal foundation, as recommended by DNV (2016).

The effects of the soil strength heterogeneity ratio and foundation embedment are shown in Figs. 6 and 7, respectively. Since h_0 is affected only by s_{u0} for surface foundations, h_0 remains to be unity regardless of the value of κ. Fig. 6

shows that the difference for v_0 (around 8.5%) between octagonal and circular foundations is approximately the same, while the difference of m_0 (around 11.4%) gradually increases with the value of κ. In Fig. 7, the embedded foundations in a homogeneous soil (i.e., κ=0) have been considered. As can be seen from Fig. 7, octagonal foundations have larger uniaxial bearing capacity factors than circular foundations. In addition, the difference of h_0 between octagonal and circular foundations appears to be smaller than that of v_0 and m_0. Relationships between the bearing capacity factors and κ and d/D are proposed in Eqs. (3) and (4). The comparison shown in Figs. 6 and 7 suggests good fits.

$$v_0 = 6.45 + \frac{15.30\kappa}{\kappa+16.82}$$
$$m_0 = 0.68 + \frac{1.44\kappa}{\kappa+19.82} \quad (3)$$

$$v_0 = 6.45 + \frac{4.17d/D}{d/D+0.49}$$
$$h_0 = 3.35\,d/D + 1.05 \quad (4)$$
$$m_0 = 0.68 - \frac{0.74d/D}{d/D-1.13}$$

Fig. 6 Uniaxial bearing capacities for surface foundations: (a) V_{ult} and (b) M_{ult}

Fig. 7 Uniaxial bearing capacities for embedded foundations: (a) V_{ult}; (b) H_{ult} and (c) M_{ult}

3.2 Horizontal-Vertical loading

The dimensionless and normalized *HV* failure envelopes for various soil heterogeneity ratios and foundation embedment ratios are depicted in Fig. 8. It can be seen from Fig. 8(a) and (c) that the absolute size of the envelope (i.e. dimensionless) increases with increasing κ and d/D. Since the size of the failure envelope is controlled by the uniaxial bearing capacities, octagonal foundations have larger dimensionless envelopes than the corresponding circular foundations. The normalized failure envelopes shown in Fig. 8(b) and (d) indicate that the *HV* envelopes normalized by the corresponding ultimate capacities collapse into a relatively narrow band, although a slight dependence on κ and d/D is observed.

A curve fit to Green's exact solution (Green 1954) is widely used to characterize the *HV* failure envelopes, as shown by Eq. (5). The comparison shown in Fig. 8(b) and (d) indicates that Eq. (5) can provide conservative predictions of the FE results. For simplicity, Eq. (5) is used to model the current *HV* failure envelopes, ignoring the slight dependence on κ and d/D.

$$V/V_{\text{ult}} = 0.5 + 0.5\sqrt{1 - H/H_{\text{ult}}}, \text{ for } V/V_{\text{ult}} \geq 0.5$$
$$H/H_{\text{ult}} = 1, \text{ for } V/V_{\text{ult}} < 0.5 \quad (5)$$

Fig. 8 *HV* failure envelopes: (a) Dimensionless, surface foundations; (b) Normalized, surface foundations; (c) Dimensionless, embedded foundations and (d) Normalized, embedded foundations

3.3 Moment-Vertical loading

Fig. 9 shows the effects of κ and *d*/*D* on the *MV* failure envelopes. Significant expansion of the failure loci with increasing κ and *d*/*D* (see Fig. 9(a) and (c)) is observed. It can be seen that the dimensionless envelopes for octagonal foundations are consistently larger than those for the corresponding circular foundations. The comparison also shows that the difference between octagonal and circular foundations for various values of κ is larger than that for different values of *d*/*D*. In addition, the difference between octagonal and circular foundations slightly increases with κ.

As shown in Fig. 9(b), the failure envelopes for the cases with different values of κ in terms of loads normalized by their ultimate values fall in a very tight band, with the shape following the parabolic function given by Eq. (6):

$$M/M_{\text{ult}} = 4[V/V_{\text{ult}} - (V/V_{\text{ult}})^2] \quad (6)$$

However, as can be seen from Fig. 9(d), the dependence of the *MV* failure envelopes on *d*/*D* cannot be directly eliminated by the normalization using the ultimate values, since an embedded foundation can still resist moment loads in the absence of vertical loads due to the side and top soils. In order to transform these failure envelopes with non-zero intercepts with the moment axis (i.e. at $V/V_{\text{ult}} = 0$) into curves that pass through the origin, the failure envelopes shown in Fig. 9(d) are shifted to the right along the *x* axis (see Fig. 10(a)), which is equivalent to:

$$V' = V + \Delta V \text{ and } V'_{\text{ult}} = V_{\text{ult}} + \Delta V \quad (7)$$

where ΔV represents the amount of offset and can be defined as $\Delta V = V_{\text{ult}} \cdot f(d/D)$, where $f(d/D)$ is a function of *d*/*D*. Curve fitting shows that $f(d/D) = 4.95(d/D)^3$ can be a satisfactory prediction. As compared in Fig. 10(b), the modified normalized *MV* failure envelopes (i.e. $M/M_{\text{ult}} \sim V'/V'_{\text{ult}}$) can still be approximated using Eq. (6).

Fig. 9 *MV* failure envelopes: (a) Dimensionless, surface foundations; (b) Normalized, surface foundations; (c) Dimensionless, embedded foundations and (d) Normalized, embedded foundations

Fig. 10 Modified *MV* failure envelopes for embedded octagonal foundations: (a) Dimensionless and (b) Normalized

The relationships between the contact area ratio (i.e. contact area / initial contact area) and load eccentricity predicted by the FE analyses and the equivalent effective area method of Hansen (1961), which is used by DNV (2016), are shown in Fig. 11. Typical contact areas for two values of load eccentricity are also presented; areas shown in black (sticking contact) and dark grey (slipping contact) are those predicted by the FE model, while the ellipse-shaped areas with red outlines and shaded with red stripes are estimated by the effective area method. It can be seen that the effective area method based on an inscribed circle consistently underestimates the contact area, resulting in the under-prediction of the moment capacity. Similar results were reported by Taiebat and Carter (2002) for eccentrically loaded circular surface foundations.

Fig. 11 Relationship between contact area and load eccentricity

3.4 Moment-Horizontal loading

The dimensionless ultimate load-carrying capacities under combined moment and horizontal loadings for different values of κ and d/D are shown in Fig. 12. Only dimensionless failure envelopes at V/V_{ult}=0.50 are presented to show the evolution of the absolute size of the envelopes. As shown in Fig. 12, octagonal foundations consistently have larger *MH* envelopes than the corresponding circular foundations. Similar to the *MV* failure envelopes, the difference of the *MH* envelope between octagonal and circular foundations for different values of κ is larger than that for various values of d/D, and the difference slightly increases with κ (see Fig. 12(a)). Therefore, the approach of using an inscribed circle for octagonal foundations recommended by DNV (2016) tends to be more conservative for soils with larger strength heterogeneity. Fig. 12 shows that the failure envelope for a surface foundation on a uniform soil is almost symmetrical about H=0. However, the soil strength heterogeneity and foundation embedment gradually increase the degree of asymmetry (i.e. obliquity of the failure envelope) due to the cross-coupling effect between horizontal loads and moments. It should also be noted that the *MH* failure envelope tends to be right-skewed (i.e. positive skewness) with the increase of κ, while foundation embedment leads to left-skewed (i.e. negative skewness) *MH* failure envelopes.

Fig. 13 shows the *M-H* failure loci (at V/V_{ult}=0.25, 0.50 and 0.75) normalized by the corresponding maximum horizontal load and moment (i.e. intersections of the failure envelopes with the horizontal load and moment axes). Since the shape of the failure envelope varies in a quite complex manner with κ and d/D, a general form of elliptic equation given by Eqs. (8) and (9) (accounting for the effects of κ and d/D, respectively) is used to approximate the FE results. The comparison presented in Fig. 13 shows reasonable predictions.

$$(H/H_{\max})^2 + (M/M_{\max})^2 + 0.22(H/H_{\max}) \cdot (M/M_{\max}) = 1 \quad (8)$$

$$(H/H_{\max})^2 + (M/M_{\max})^2 - 0.082(H/H_{\max}) \cdot (M/M_{\max}) = 1 \quad (9)$$

Fig. 12 Dimensionless *MH* failure envelopes at V/V_{ult}=0.50: (a) Surface foundations and (b) Embedded foundations

Fig. 13 Fitting of *MH* failure envelopes: (a) Surface octagonal foundations on a non-homogeneous soil and (b) Embedded octagonal foundations in a uniform soil

4 Full 3-D failure envelope in VHM loading space

This section derives a 3-D analytical expression for the failure envelope in VHM loading space. Based on the forms of the equations used in the previous sections, more general forms of the FE-derived equations are summarized in Eq. (10). In Eq. (10), the parameter *c* governs the tilt of the *M-H* failure envelope. According to Eqs. (8) and (9), the value of *c* is positive for the case of a surface foundation on a non-homogeneous soil and negative for the case of an embedded foundation in a homogeneous soil. Specific expressions of these failure envelopes for different soil and foundation conditions can be found in the previous sections.

$$\begin{gathered} M = 0: \ H_{\max}/H_{\text{ult}} = f_h(V/V_{\text{ult}}) \\ H = 0: \ M_{\max}/M_{\text{ult}} = f_m(V/V_{\text{ult}}) \\ V \neq 0: \ (H/H_{\max})^2 + (M/M_{\max})^2 + c(H/H_{\max})(M/M_{\max}) = 1 \end{gathered} \quad (10)$$

Mathematical manipulations of Eq. (10) allow the formulation of a 3-D analytical expression for the failure envelope in VHM loading space in terms of V/V_{ult}, H/H_{ult} and M/M_{ult}:

$$\left(\frac{H/H_{\text{ult}}}{f_h(V/V_{\text{ult}})}\right)^2 + \left(\frac{M/M_{\text{ult}}}{f_m(V/V_{\text{ult}})}\right)^2 + c\left(\frac{H/H_{\text{ult}}}{f_h(V/V_{\text{ult}})}\right)\left(\frac{M/M_{\text{ult}}}{f_m(V/V_{\text{ult}})}\right) = 1 \quad (11)$$

As an example, the full 3-D expression of the failure envelope for a circular surface foundation on non-homogeneous soils is shown in Fig. 14. The expressions for the *HV*, *MV* and *MH* failure envelopes can be found in the previous sections and are also shown for comparison.

Fig. 14 3-D VHM failure surfaces for a circular surface foundation on non-homogeneous soils

5 Conclusions

The general VHM failure envelopes of octagonal foundations under a zero-tension interface for undrained soils have been studied using finite element (FE) analyses. Two sets of FE cases, i.e. surface foundations on heterogeneous soils

and embedded foundations in uniform soils, were considered to investigate the effects of soil strength heterogeneity and foundation embedment. Analytical formulas have been proposed to calculate the uniaxial capacities and the *VH*, *VM* and *MH* failure envelopes. The results indicate that the failure envelopes for octagonal foundations have similar shapes to those for the inscribed circular foundations. However, the size of the failure envelopes for octagonal foundations is larger, and the difference (about 10%) between them is not negligible. Therefore, the approximate method recommended for octagonal foundations by some design guidelines can be seen to be conservative. To facilitate the use of the developed method for the design of octagonal foundations, a full 3-D analytical expression for the VHM load failure envelope was derived based on the results provided herein. These approaches should aid the assessment of the ultimate limit state of shallow octagonal foundations under complex VHM loading conditions.

6 Acknowledgements

The authors would like to acknowledge the financial support of Natural Sciences and Engineering Research Council of Canada (Grant No.: RGPIN-2015-06062).

References

Abyaneh SD, Ojo A, Maconochie A, Haghighi A (2015) The undrained bearing capacity of shallow foundations subjected to three-dimensional loading including torsion. *In* Proceedings of the 25th International Ocean and Polar Engineering Conference, Kona, Hawaii, 21-26 June 2015. International Society of Offshore and Polar Engineers, Cupertino, pp. 668-674.

API RP 2GEO (2011) API Recommended Practice, Geotechnical and Foundation Design Considerations. American Petroleum Institute, Washington, USA.

Dassault Systèmes (2016) Abaqus analysis user's manual. Simulia Corp. Providence, USA.

Deshpande VM (2016) Numerical Modelling of Wind Turbine Foundations subjected to Combined Loading. Dissertation, The University of Western Ontario.

DNV GL, DNVGL-ST-0126 (2016) Support structures for wind turbines. DNV GL, Oslo, Norway.

Ganesh R, Kumar J (2021) Ultimate bearing capacity of strip and circular foundations using power type yield criterion using the method of stress characteristics. Comput Geotech 133: 104066. https://doi.org/10.1016/j.compgeo.2021.104066.

Gourvenec S (2007) Shape effects on the capacity of rectangular footings under general loading. Géotechnique 57(8): 637-646. https://doi.org/10.1680/geot.2007.57.8.637.

Gourvenec S, Randolph M (2003) Effect of strength non-homogeneity on the shape of failure envelopes for combined loading of strip and circular foundations on clay. Géotechnique 53(6): 575-586. https://doi.org/10.1680/geot.2003.53.6.575.

Gourvenec SM, Mana DSK (2011) Undrained vertical bearing capacity factors for shallow foundations. Géotechnique Letters 1(4): 101-108. https://doi.org/10.1680/geolett.11.00026.

Green AP (1954) The plastic yielding of metal junctions due to combined shear and pressure. J Mech Phys Solids 2(3): 197-211. https://doi.org/10.1016/0022-5096(54)90025-3.

Hansen JB (1961) A general formula for bearing capacity. Bulletin No. 11, Danish Geotechnical Institute, Copenhagen, Denmark, 38-46.

He P, Newson T (2019) Undrained capacity of circular foundations under combined horizontal and torsional loads. Geotech Lett 10: 1-5. https://doi.org/10.1680/jgele.19.00016.

ISO (International Standards Organisation) (2016) Petroleum and natural gas industries specific requirements for offshore structures – part 4: geotechnical and foundation design considerations, 2nd edition. International Standards Organisation, Geneva, Switzerland.

Shen Z, Feng X, Gourvenec S (2016) Undrained capacity of surface foundations with zero-tension interface under planar VHM loading. Comput Geotech 73: 47-57. https://doi.org/10.1016/j.compgeo.2015.11.024.

Shen Z, Feng X, Gourvenec S (2017) Effect of interface condition on the undrained capacity of subsea mudmats under six-degree-of-freedom loading. Géotechnique 67(4): 338-349. https://doi.org/10.1680/jgeot.16.P.097.

Suryasentana SK, Dunne HP, Martin CM, Burd HJ, Byrne BW, Shonberg A (2020) Assessment of numerical procedures for determining shallow foundation failure envelopes. Géotechnique 70(1): 60-70. https://doi.org/10.1680/jgeot.18.P.055.

Taiebat HA, Carter JP (2002) Bearing capacity of strip and circular foundations on undrained clay subjected to eccentric loads. Géotechnique 52(1): 61-64. https://doi.org/10.1680/geot.2002.52.1.61.

Taiebat HA, Carter JP (2010) A failure surface for circular footings on cohesive soils. Géotechnique 60(4): 265-273. https://doi.org/10.1680/geot.7.00062.

Ukritchon B, Whittle AJ, Sloan SW (1998) Undrained limit analyses for combined loading of strip footings on clay. J Geotech Geoenviron Eng 124(3): 265-276. https://doi.org/10.1061/(ASCE)1090-0241(1998)124:3(265).

Wang Y, Cassidy MJ, Bienen B (2020) Numerical investigation of bearing capacity of spudcan foundations in clay overlying sand under combined loading. J Geotech Geoenviron Eng 146(11): 04020117. https://doi.org/10.1061/(ASCE)GT.1943-5606.0002369.

Yilmaz M, Schubert S, Tinjum JM, Fratta D (2014) Foundation soil response to wind turbine generator loading. *In* Geo-Congress 2014: Geo-characterization and Modeling for Sustainability, Atlanta, Georgia. 23-26 February 2014. American Society of Civil Engineers, New York, pp. 1493-1502.

Statements and Declarations

Funding

This work was supported by the Natural Sciences and Engineering Research Council of Canada (Grant number RGPIN-2015-06062).

Competing Interests

The authors have no relevant financial or non-financial interests to disclose.

Author Contributions

Conceptualization: Pengpeng He and Tim Newson; Methodology: Pengpeng He and Venkatesh Deshpande; Formal analysis and investigation: Pengpeng He; Writing - original draft preparation: Pengpeng He; Writing - review and editing: Venkatesh Deshpande and Tim Newson; Funding acquisition: Tim Newson; Supervision: Tim Newson.

Data Availability

The datasets generated during the current study are available from the corresponding author on reasonable request.

List of Figures

Fig. 1 LRP and soil strength profile

Fig. 2 Mesh convergence study for a homogeneous soil

Fig. 3 Half-view of the FE mesh

Fig. 4 Sign conventions

Fig. 5 *MH* failure envelopes of a surface foundation for κ=0 at V/V_{ult}=0.50

Fig. 6 Uniaxial bearing capacities for surface foundations: (a) V_{ult} and (b) M_{ult}

Fig. 7 Uniaxial bearing capacities for embedded foundations: (a) V_{ult}; (b) H_{ult} and (c) M_{ult}

Fig. 8 *HV* failure envelopes: (a) Dimensionless, surface foundations; (b) Normalized, surface foundations; (c) Dimensionless, embedded foundations and (d) Normalized, embedded foundations

Fig. 9 *MV* failure envelopes: (a) Dimensionless, surface foundations; (b) Normalized, surface foundations; (c) Dimensionless, embedded foundations and (d) Normalized, embedded foundations

Fig. 10 Modified *MV* failure envelopes for embedded octagonal foundations: (a) Dimensionless and (b) Normalized

Fig. 11 Relationship between contact area and load eccentricity

Fig. 12 Dimensionless *MH* failure envelopes at V/V_{ult}=0.50: (a) Surface foundations and (b) Embedded foundations

Fig. 13 Fitting of *MH* failure envelopes: (a) Surface octagonal foundations on a non-homogeneous soil and (b) Embedded octagonal foundations in a uniform soil

Fig. 14 3-D VHM failure surfaces for a circular surface foundation on non-homogeneous soils